The fruit of the first two years of the project (2018-2019) is the article titled as **"Spinal Excitatory Dynorphinergic Interneurons Contribute to Burn Injury-Induced Nociception Mediated by Phosphorylated Histone 3 at Serine 10 in Rodents"** published in Int J Mol Sci (DOI: 10.3390/ijms22052297).

In this work, we combined immunohistochemistry, in situ hybridization with the retrograde labeling of projection neurons to reveal the subset of dorsal horn neurons presenting an elevated level of p-S10H3 in response to noxious heat (60 °C), causing burn injury.

Main results of the article referred to above:

- p-S10H3 expression is upregulated in a subpopulation of ipsilateral spinal dorsal horn (SDH) neurons with differing rostrocaudal density following burn injury
- SDH neurons expressing p-S10H3 following burn injury are in close apposition mainly to CGRP-containing peptidergic afferents
- S10H3 phosphorylation occurs predominantly in SDH neurons in mice
- only a small proportion of projection neurons expresses nuclear p-S10H3 following burn injury
- percentage of p-S10H3+ neurons after burn injury that were Pax-2 or Lmx1b-immunoreactive (IR) in wild type mice or that were VGAT- or vesicular glutamate transporter 2 (Vglut2)-IR in VGAT- or Vglut2:tdTomato transgenic mice.
- by combining ISH for Tac1 or GRP RNAs with immunostaining for p-S10H3, we provided evidence that none of these excitatory neurons are involved in the p-S10H3-mediated pathway following burn injury and consequential tissue damage.
- burn injury-induced S10H3 phosphorylation occurs mainly in a dynorphinergic (Pdyn) of SDH neurons in mice
- a dedicated subset of excitatory dynorphinergic neurons is likely a key player in the development of central sensitization via the p-S10H3 mediated pathway.

Based on these findings we hypothesized that blocking histone H3.1 phosphorylation at position serine 10 (S10) Pdyn-selectively in the spinal dorsal horn neurons of mice would reduce or even eliminate central sensitization and consequent inflammatory hyperalgesia induced by noxious heat or in the absence of prior painful stimulus would cause anti-nociception. Thus, in the last period of the study (2020-2021), to test our hypothesis that S10H3 plays a critical role in nociceptive processing in the spinal dorsal horn of transgenic mice CRISPR/cas9 genome editing technology was utilized. We used intrathecal administration of recombinant adeno-associated virus (rAAV9) encoding CRISPR/cas9 components targeting the wild-type histone H3.1 in näive transgenic mice to investigate the effect of serine exchange to alanine at position 10 of histone H3.1 (S10A) on thermal- and mechanical thresholds as well as on formalin-induced chemonociception.

These findings provided an answer to what extent dynorphinergic neurons, in which S10H3 is phosphorylated upon noxius stimulus, contribute to thermonociception and whether inhibition of S10 phosphorylation on histone H3.1 can indeed lead to impaired heat perception.

Manuscript dealing with these findings has been submitted to the Progress in Neurobiology, which is ranked as Q1 journal in Neuroscience, and titled as "**CRISPR/cas9-based mutagenesis of histone H3.1 in spinal dynorphinergic neurons attenuates thermal sensitivity in mice**" (manuscript number: PRONEU-D-21-00425) and presented here as follows:

Abstract

Burn injury is a trauma resulting in tissue degradation and severe pain, which is processed first by neuronal circuits in the spinal dorsal horn. We have recently shown, that in mice, excitatory dynorphinergic (Pdyn) neurons play a pivotal role in the response to burn injury-associated tissue damage, via histone H3.1 phosphorylation-dependent signaling. As Pdyn neurons were mostly associated with mechanical allodynia, their involvement in thermonociception had to be further elucidated.

Using a custom-made AAV9_mutH3.1 virus combined with the CRISPR/cas9 system, here we provide evidence that blocking histone H3.1 phosphorylation at position serine 10 (S10) in spinal Pdyn neurons significantly increases thermal nociceptive threshold in mice. In contrast, neither mechanosensation nor acute chemonociception was affected by the transgenic manipulation of histone H3.1.

These results suggest that blocking rapid epigenetic tagging of S10H3 in spinal Pdyn neurons alters acute thermosensation and thus explains the involvement of Pdyn cells in the immediate response to burn injury-associated tissue damage.

1. Introduction

Neurons in the superficial dorsal horn (SDH) of the spinal cord are known to play a key role in the regulation of nociceptive information flow. Despite the increasing number of neuroepigenetic studies in pain research, the molecular mechanisms involved in the processing and differentiating of painful modalities are not well characterized. While some posttranslational modifications (PTM), e.g. histone H3.1 acetylation, in the maintenance of pathological pain has been already studied in detail, (Liang et al., 2014; Descalzi et al., 2015; Liang and Tao, 2018) the role of other PTMs, such as phosphorylation at position serine 10 (S10) of histone H3.1 in nociception has only recently been scrutinized (S10H3; p-S10H3; Tochiki et al., 2016; Torres-Perez et al., 2017; Varga et al., 2021). Based on our previous observations, phosphorylation of the histone H3.1 protein appears to be a reliable marker of enhancement of neuronal activity in the SDH following certain noxious stimuli (Torres-Perez et al., 2017; Varga et al., 2021).

General inhibition of S10H3 phosphorylation either by pharmacological blockage of the mitogen and stress-activated kinases (MSK; Tochiki et al., 2016) or by transgenic technology (using MSK1/2 gene-deficient mice; Torres-Perez et al., 2017) prevents the development of heat hypersensitivity without affecting the development of mechanical allodynia following carrageenan-induced inflammation (Torres-Perez et al., 2017). Several recent studies showed that somatosensory modalities are likely to be processed by definite but somewhat overlapping interneuronal populations in the SDH (Brewer et al., 2020; Duan et al., 2014; Petitjean et al., 2015). Of these inhibitory subgroups, dynorphinergic (Pdyn) neurons are regarded to be primarily responsible for the gating of mechanical and pruritic pain (Brewer et al., 2020; Duan et al., 2014; Huang et al., 2018; Kardon et al., 2014). We have recently reported that spinal excitatory Pdyn neurons have a major contribution to the response to burn-injury associated tissue injury, via p-S10H3-dependent signaling (Varga et al., 2021). Therefore, we hypothesized that specific blocking of histone H3.1 phosphorylation at position serine 10 (S10) in spinal Pdyn neurons alone would reduce or even eliminate central sensitization and heat hypersensitivity, consequently leading to a certain level of anti-nociception. In situ genetic manipulation of histone H3.1, however, is quite challenging due to its redundancy in the genome and its essential function during the mitosis of the cell cycle. To overcome this obstacle and test our hypothesis that p-S10H3 plays a critical role in the processing of noxious heat-associated pain, in this study, we designed a recombinant adeno-associated virus (AAV9) based expression vector that combines dominant-negative and CRISPR/cas9 technology. The vector induces expression of a mutant histone H3.1 in which serine is replaced with alanine at position 10 (S10A) and also CRISPR elements for targeted deletion of the wild type histone H3.1 genes. Intrathecal application of our AAV9 construct revealed that Pdyn neuron selective inhibition of S10 phosphorylation on histone H3.1, leads to a significant increase of the thermal nociceptive threshold, while leaves perception of other modalities intact.

2. Material and Methods

2.1. Animals and ethical considerations

Animal experiments were approved by the Animal Care and Protection Committee at the University of Debrecen (No.: 23-1/2017/DEMÁB) and were performed along with the European Community Council Directives and the IASP Guidelines. Animals were housed individually in a temperature-controlled colony room and maintained on a 12h/12h light/dark cycle. Food and water were provided ad libitum. Pdyn-IRES-Cre mice (see Key resources provided in Supplementary Table S1) which express Cre recombinase under the direction of the Pdyn (prodynorphin) promoter (Krashes et al., 2014) were crossed with Rosa26-LSL-Cas9 (Supplementary Table S1) knockin mice having Cre-dependent expression of CRISPR associated protein 9 endonuclease (cas9) and enhanced green fluorescent protein (EGFP) directed by a CAG promoter (Platt et al., 2014). Genotyping of litters from both strains was routinely performed by PCR (for primer sequences see Supplementary Table S2). In the resulting hybrid mice (Pdyn::cas9-EGFP) all Pdyn-containing neurons showed strong somatic EGFP expression in the brain (Fig. 1) as well as in the spinal cord (Fig. 2a; Fig. 4). Adhering to the 3R principle (replacement, reduction, refinement) altogether 19 adult male mice (between 26.2g-34.1g; 17 Pdyn::cas9-EGFP hybrids and 2 wild type C57BL/6 mice). All the mice underwent surgical intervention, either cannulation for the osmotic pump or sham operation.

2.2. Designing the construct containing the mutant histone H3.1 and CRISPR elements

The dominant-negative mutant S10A H3.1 coding sequence, multiplex single guiding RNAs (sgRNAs), and even a fluorescent reporter gene was incorporated into the all-in-one AAV construct. The dominant-negative sequence including the complete histone H3.1 sequence with serine to alanine point-mutation at position S10 (S10A; mutH3.1) driven by a strong synthetic hybrid CMV enhancer/chicken β-actin (CBh) promoter was incorporated into a pCBh cloning vector in silico using SnapGene software (from Insightful Science; available at snapgene.com). Both ends of this template sequence contained loxP sites ensuring cre-dependent transcription of mutH3.1. Thus, in addition to cas9 expression provided by the transgenic line applied, the expression of the mutant H3.1 template was also restricted to Pdyn neurons due to their cre dependency.

For multiplex CRISPR/cas9-based genome editing, a human U6 small nuclear promoter was chosen to express three different sgRNAs targeting the same gene (histone H3.1 gene) in a single expression cassette. sgRNA sequences targeting wild-type histone H3.1 are shown in Supplementary Table S3.

Additionally, mCherry fluorescent coding sequence under the control of constitutive CMV promoter was also incorporated behind the mutH3.1_sgRNA cassette without adding loxP sites. This way, the cre-independent expression of mCherry allowed verification of the viral infection by detecting the immunohistochemically enhanced red signal with fluorescent microscopy. The final construct (Fig. 2c), which contained the mCherry sequence and the mutH3.1_sgRNA cassette, was flanked by BamHI restriction sites in both ends. Its total length was 4,399 bp. This insert was then synthesized and cloned into a commonly used cloning vector pUC57 by GenScript. Complete insert sequences with color codes are found in Supplementary Data S1. This final insert in pUC57 plasmid was packaged into serotype 9 recombinant adeno-associated virus vector (AAV9) and purified for in vivo application by SignaGen Laboratories (titer >1E+13 VG/mL) resulting in AAV9_mutH3.1.

2.3. Intrathecal administration of the viral vector

Experimental design is illustrated schematically in Fig. 2b. Pdyn::cas9-EGFP hemizygous hybrids were injected intrathecally (IT) with the AAV9_mutH3.1 containing the mutH3.1_sgRNA cassette plus the mCherry sequence. The viral suspension was administered continuously through an osmotic pump which had been connected to an intrathecal catheter. Before the implantation pumps were soaked in sterile 0.9% saline for a couple of hours to promote the priming procedure. Under the fume-hood pumps were filled with the viral solution in a final volume of 100 µl in a titer of 3E+9 VG/mL using a cut-ended pipette microtip. Till the insertion of the osmotic pump, the pump reservoir was placed in an upright position into an Eppendorf tube to avoid evaporation of the solution from the pump. The release rate for the applied ALZET pump model (003D) was 1µl/hr and the duration of the complete release was 3 days.

After induction of anesthesia using intraperitoneal administration of sodium-pentobarbital (<50mg/kg), each mouse was placed in a prone position. The skin on the back of the animal was shaved and disinfected with 70% ethanol and an incision in the midline was performed. For intrathecal cannulation, the tip of a 26G needle was gently inserted at about 90° angle, into the L4-L5 intervertebral space in the midline. As soon as the tip of the needle passed through the dura mater, the characteristic tail-flick reflex could be observed. Next, the angle of the needle was decreased to about 30° and slightly pushed rostrally for 1-2 mm in the subarachnoidal space. The needle was replaced by a polyurethane mouse intrathecal catheter including a Teflon coated stylet for easier placement. After validating the correct position of the catheter in the intrathecal space by microCT or X-ray, the cannula was attached to the Alzet osmotic pump which had been filled with the viral solution. The wound was sutured and the mice were allowed to fully recover. Three days after the surgery, both the pump and the catheter were removed from the re-anesthetized animals.

2.4. Control groups

Three sets of controls were included in this study. In the first control group, referred to as "AAV9_control" throughout the text, Pdyn::cas9-EGFP mice (n=6) were injected with an irrelevant, but AAV9-derived viral vector (pAAV-EF1a-double floxed-hChR2(H134R)-mCherry-WPRE-HGHpA; from Karl Deisseroth). The animals underwent the same surgical procedures (see in chapter 2.3.) and received the irrelevant virus in the same titer as the AAV9_mutH3.1. The second control group contained sham-operated Pdyn::cas9-EGFP mice (n=4), while in the third control group wild-type C57/B6 mice were treated with the AAV9_mutH3.1 (n=2). Animals in the sham-operated control group underwent the same surgical intervention as described above. The only difference was that the osmotic minipump has not been attached to the catheter. Anesthesia, skin incision, insertion of the catheter, and even the re-operation on the third day to simulate removal of the catheter were the same.

2.5. Verification of the position of the intrathecal catheter by 3D micro-computed tomography (micro-CT)

The SkyScan 1272 compact desktop micro-CT system was used to determine the location of the intrathecal catheter in deeply anesthetized mice (Fig. 2d), using the following scanning parameters: image pixel size, 26 µm; matrix size, 672 × 1008 (rows × columns); source voltage = 60 kV; source current = 166 µA; rotation step (deg) = 0.300, filter = Al 0.25mm. Flat field correction and geometrical correction were applied to the images. Scan duration: 0h:28m:19s. Reconstruction of the cross-sectional images from tomography projection images was performed with the SkyScan NRecon software (version 2.0.4.2). Post-alignment, beam hardening correction, ring artifact correction, and smoothing were completed during post-processing of the image data. The output formats were DICOM and BPM images. The 3D Volume rendering tool provided by RadiAnt DICOM Viewer was utilized to visualize 3D micro-CT images (Fig. 2d). Micro-CT validation of catheter position was performed in the case of the first 5 interventions. Since ionizing radiation was hinted to influence the experimental outcome (Willekens et al., 2010), in the case of the remaining mice the verification of catheter position was performed with conventional X-ray imaging to reduce the dose load. The average estimated dose load was 125 mGy (lethal dose in mice ranges are from 5.0 to 7.6 Gy, depending on the strain and age; (Kohn and Kallman, 1957; Sato et al., 1981).

2.6. Thermal sensitivity assessments

Response latency to noxious heat (50 °C) was evaluated using a hot plate test. Before testing mice were preconditioned for the hot plate every day for a week before, and on every second day after the surgical implantation of the osmotic pump. During preconditioning, animals were placed onto the hot plate, which was set to an innoxious surface temperature (37 °C), for approximately 10 minutes. Thermal response latency was determined by an independent observer who was blind to the treatment. When the animal exhibited discomfort upon constant high temperature (i.e. sudden lifting/withdrawal, licking, or shaking the affected hindlimb) the heating of the surface was immediately terminated and the response latency (sec) was noted. The maximum cutoff latency was set to 50 sec to prevent burn injury of the paw. Response latencies to noxious heat were assessed in a three-day window before (BTM; baseline threshold measurement; Fig. 3a) and on days 7th, 14th, and 21st after the osmotic pump implantation (Fig. 3a; 3b). Since a distinct disadvantage of the hot plate test is its sensitivity to repeated measurements, likely via learning (Espejo et al., 1994; Milne et al., 1989; Plone et al., 1996), we only took a single measurement in the case of each animal at a given time point. The averaged response latencies from the animals on each measurement day were normalized to baseline latencies (the value shown for day 0) and displayed as percentages.

2.7. Mechanical sensitivity assessments

Tactile sensitivity was measured as paw withdrawal latency (PWL) to dynamic von Frey stimulation (Schmidtko et al., 2008), at the same timepoints as the hot plate tests. The maximum force used was 5 g (increasing between 0.8–5 g) with 10-sec intervals between trials, performed by two independent observers who were blind to the treatment. The withdrawal latencies on each measurement day (day 7, 14, 21 after the osmotic pump implantation) were normalized to baseline withdrawal latencies (day 0) and displayed as percentages.

2.8. Formalin-induced acute somatic nocifensive behavior

Following the 3-week post-implantation period (see Fig. 3a), rapid inflammation-induced pain was evoked by injecting formalin (5% of Formaldehydum solution 37%; Ph.Hg. VII.; in a volume of 25 ul; i.pl.) into the right hind paw of sham-operated or Pdyn::cas9-EGFP hybrid mice which had been injected with one of the viruses (AAV9_mutH3.1or AAV9_control). Animals were then immediately placed into a 17x17-cm plexiglass observation chamber equipped with a mirror in the back, and formalin-induced nocifensive behavior was recorded with the camera, continuously for one hour.

Nocifensive behavior was assessed as the length of time spent lifting, licking, or shaking the treated hind paw in 5-minute periods across 60 min. Evaluation of the experiments was done with an experimenter blinded to the treatment. The contralateral leg was omitted from the observation. Formalin-induced somatic chemonocifensive response appears in two phases (Bolcskei et al., 2005; Tjolsen et al., 1992). Due to transient and rapid activation of sensory nerve endings the early phase lasts only 5-15 min, while the late phase (15-60 min) is generated by the release of acute inflammatory mediators (Tjolsen et al., 1992). The duration of nocifensive behavior was measured in both periods (Bolcskei et al., 2005).

2.9. Tissue preparation for microscopic analysis

Sampling and tissue processing were performed as described previously (Varga et al., 2021). After inducing non-recoverable anesthesia with sodium pentobarbital (50 mg/kg intraperitoneal) animals were transcardially perfused with 4% paraformaldehyde (PFA). The brain and the lumbar spinal cord were removed and sectioned with a vibratome (Leica CLS 100X) at 150 and 100 µm thickness, respectively.

2.10. Immunoperoxidase staining

For mapping the supraspinal distribution of Pdyn neurons in Pdyn::cas9-EGFP mice, the whole brain was removed and sectioned. After quenching endogenous peroxidase activity with Dent's bleach (methanol:DMSO:H_2O_2 in a ratio of 8:1:1), an antibody raised against GFP (Suppl. Table S1) was added to the samples (1:4000; 2 days). Two-hour-long incubation with the secondary antibody (1:500; room temperature) was followed by adding extravidin (1:500) to the specimen. All reactions were carried out overnight at 4°C unless otherwise stated. Finally, the DAB peroxidase substrate kit was used for the visualization of the GFP-positive signal. Sections were counterstained with Toluidine blue and mounted in Eukitt mounting medium. Reagents are summarized in Suppl. Table S1. The location of the Pdyn neuronal somata, containing DAB precipitate was noted with the Neurolucida software (v11.07) in randomly selected slices (n=8), using x10 objective lens (Olympus).

2.11. Visualization of mCherry expression in the lumbar spinal cord by immunofluorescent staining for confocal imaging

Cells infected with the AAV9_mutH3.1 were identified based on their mCherry expression. Confocal microscopic analyses were performed on transverse lumbar spinal cord sections as detailed in our previous study (Varga et al., 2021) with slight modifications. Briefly, a primary antibody mixture was applied on sections (overnight; 4 °C), which contained chicken anti-GFP (1:2000) and rat anti-RFP (1:1000; see details in Supplementary Table S1) to enhance the native fluorescent signals. Cell nuclei-specific DAPI and species-specific secondary antibodies raised in donkey conjugated to Alexa Fluor-488 or 555 (see in Supplementary Table S1) were added to the sections for 2 hrs at room temperature at the end of the immunofluorescence staining protocol. All antibodies were diluted in phosphate-buffered saline (PBS) supplemented with a 0.3% Triton-X 100. Sections were mounted in a Hydromount medium and confocal images were scanned with Olympus FV3000 confocal systems.

Confocal images were acquired with the same settings (PMT voltage, laser transmissivity, Z dimension parameters, etc.). Using ×10 lens (UPlanSApo, Olympus, N.A. 0.4), confocal image stacks consisting of 4 optical images at 3.6 µm z-separation. In some cases, for higher magnification with x40 objective lens (UPlanFLN, Olympus, N.A. 1.3), 16 optical sections of 0.5 µm thickness were acquired unless otherwise indicated. Post-processing of the images was done with the FV31S-DT software (see software details in Supplementary Table S1).

2.12. Detection of mCherry mRNA and the mutant variant of histone H3.1 transcripts in the spinal cord

Five weeks after IT injection of rAAV9_mutH3.1 into a wild-type mouse, total RNA was extracted from the harvested lumbar segment of the spinal cord and from the hippocampus using TRIzol reagent (see in Supplementary Table S1). Total RNA was reverse transcribed and specific fragments (mCherry and GAPDH) from cDNA were amplified with DreamTaq DNA Polymerase (Thermo Fisher Scientific) according to manufacturers' recommendations. The primer sets were designed by using Primer3Plus and are shown in Supplementary Table S2.

2.13. Statistical analysis

Detailed statistical analyses for the data presented in Fig. 3. can be found in Supplementary Table S4. The PWL values and values for body weight were normalized to the baseline level (BTM; baseline threshold measurements; considered to be the same on day 0) and expressed as percentages. All normalized data were averaged and presented in the relevant figures as mean ± standard error of mean (SEM) of n = 3–7 mice per group (see Supplementary Table S4). Statistical analysis for the third control group (wild-type C57/B6 mice were treated with the AAV9_mutH3.1) was neglected due to the low number of animals included in the experiment (n=2).

The Kruskal-Wallis non-parametric ANOVA test with Origin Pro9 software was applied to determine the overall significance of the treatment on paw withdraw latency in response to noxious heat/mechanical force or on body weight (raw values were applied for analysis).

With the aid of Origin Pro9, the Mann-Whitney U test was used to compare the three experimental groups with each other (AAV9_mutH3.1; AAV9_control; sham group) at each measurement point (normalized values were applied for comparison).

In the case of the formalin test, the overall influence of each treatment on the 1st and 2nd phases of formalin response was evaluated by the Kruskal-Wallis non-parametric ANOVA test.

In all cases $p<0.05$ or $p<0.01$ were accepted as statistically significant as indicated in the relevant figures.

3. Results

3.1. Distribution of dynorphinergic neurons in various brain regions of the Pdyn::cas9-EGFP hybrid mouse

Somatic visualization of certain types of neuropeptides following standard immunostaining procedure often suffers from significant detection problems due to biosynthetic and trafficking characteristics of those molecules (Hook et al., 2008; Huang et al., 2008; Marvizon et al., 2009; Sardella et al., 2011; van den Pol, 2012). To overcome this problem in the case of dynorphin, several solutions have been developed and utilized recently. Antibodies raised against the dynorphin precursor preprodynorphin (PPD), in situ hybridization (ISH), or even genetically engineered transgenic animals are all available to label cells selectively with a knocked-in fluorescent tag (Baseer et al., 2012; Doyle et al., 2012; Krashes et al., 2014; Platt et al., 2014; Sapio et al., 2020; Sardella et al., 2011; Varga et al., 2021).

In the hybrid, that we used throughout the study, Pdyn expression is linked to cas9-EGFP due to the cre-dependence of cas9. Thus, Pdyn could be identified based on their EGFP expression in this animal. To confirm the reliability of EGFP expression in Pdyn neurons we used conventional immunohistochemistry on coronal sections of the whole brain (Fig. 1 & Suppl. Fig. S1). Neurolucida reconstruction of the location of EGFP positive cell bodies, after HRP-DAB conversion, proved that the great majority of DAB+ cells was restricted to those areas which have been designated as dynorphinergic neurons rich areas in the Allen Brain Atlas by ISH (ABA, www.brain-map.org; (Lein et al., 2007) (Fig. 1). This finding confirmed that the hybrid selected for the experiments is indeed suitable for cas9-based manipulation of dynorphinergic neurons and also for the selective insertion of S10A into Pdyn-expressing neurons exclusively.

In addition, we observed a high level of co-localization between the antibodies against the neuropeptide precursor preprodynorphin (PPD) and the EGFP signal in the superficial laminae of the spinal dorsal horn (SDH; Fig. 2a) from a Pdyn::cas9-EGFP mouse, whereas, in deeper laminae, where mainly excitatory Pdyn neurons are present (Boyle et al., 2017; Sardella et al., 2011), EGFP-immunoreactive neurons lacked Pdyn (Fig. 2a).

Given that EGFP+/Pdyn- neurons were more numerous in the deeper dorsal horn laminae of the spinal cord in adult mice, those of neurons probably transiently expressed Pdyn at an earlier stage of their development. This might also be true for some of the supraspinal regions where abundant EGFP expression was detected. This hypothesis, however, could not be confirmed from the ABA (Fig. 1 & Suppl. Fig. S1).

3.2. Validation of our experimental strategy

Schematic representation of our experimental design and the final insert which was synthesized and cloned into an adeno-associated viral vector serotype 9 (AAV9) are illustrated in Fig. 2b and 2c, respectively. Prior to the osmotic pump implantation, the position of the intrathecal catheter was confirmed in the case of each animal with either micro-computed tomography (micro-CT) or conventional X-ray (see also in Methods; Fig. 2d). Using RT-PCR, we confirmed the presence of the mCherry mRNA in the spinal cord, but not in the hippocampus of wild type mouse that had been transfected with the AAV9_mutH3.1 (Fig. 2e) indicating that the intrathecal route of AAV9 delivery results in not only efficient but also spatially restricted transduction of spinal cord neurons (Suppl. Table S2).

3.3. Intrathecal administration of AAV9_mutH3.1 virus into Pdyn::cas9-EGFP mice increases the thermal nociceptive threshold

Although prior works have reported that dynorphinergic neurons in SDH do not contribute to heat sensation in mice (Brewer et al., 2020; Duan et al., 2014), our previous findings demonstrated that excitatory dynorphinergic neurons exhibited phosphorylation of S10H3 shortly after noxious heat-induced burn injury. Therefore, to evaluate their role in thermosensation, the thermal nociceptive threshold was determined using a hot plate with constant temperature (50 °C) in a set of in vivo experiments. AAV9_mutH3.1 or AAV9_control vectors were administered via intrathecal route into the subarachnoid space of Pdyn::cas9-EGFP hybrid and wild-type mice (Fig. 3a; b). The thermal nociceptive threshold was measured before (BTM; baseline threshold measurement) and after the osmotic pump installation (days 7, 14, and 21; Fig. 3a; b).

The elevation in thermal nociceptive latency (represented as paw withdrawal latency; PWL) was most pronounced by the end of the first week (measured on day 7) after osmotic pump implantation in the group of AAV9_mutH3.1-treated mice (to 243.7%±28.4) as compared to the baseline (Fig. 3b). The elevation, although less pronounced, remained significant throughout the 3-week observational period. At each time point after the infection, AAV9_mutH3.1-treated Pdyn::cas9-EGFP hybrid mice exhibited significantly higher thermal withdrawal latencies compared to values of the hybrid animals infected with the AAV9_control virus or the sham-operated groups (see Supplementary Table S4). The average paw withdrawal latencies (PWL) in the AAV9_mutH3.1 treated mice before (BTM) and after (day 7) the infection was 15.0±1.7 sec and 33.8±3.3 sec (n=7), respectively; while the corresponding values of the AAV9_control mice were 21.7±1.1 sec and 24.9±1.3 sec (n=6), respectively.

Animals in the AAV9_control injected and sham-operated groups did not show significant alterations in PWL to noxious thermal stimulus compared to their baseline (BTM) values (Fig. 3b; for statistical analysis see Supplementary Table S4). Similar to the other control groups, wild-type mice infected with AAV9_mutH3.1 only exhibited moderate alteration in PWL (n=2). These data strongly suggest that S10H3 phosphorylation in Pdyn neurons is a crucial process for normal acute noxious heat sensation.

3.4. Intrathecal administration of AAV9_mutH3.1 virus into Pdyn::cas9-EGFP mice does not affect mechanical sensitivity

Several recent studies demonstrated that Pdyn neurons in the SDH of mice contribute to the suppression of mechanical sensation (Brewer et al., 2020; Duan et al., 2014; Huang et al., 2018). Thus, the mechanical withdrawal threshold (represented as PWL) was measured using von Frey filaments with increasing forces before and after the inhibition of S10H3 phosphorylation. PWL to noxious mechanical stimuli showed an increase on days 7 and 14 and reached 149.7%±12.0 by day 21, however, this alteration in tactile sensitivity was not statistically significant (Fig. 3c), suggesting that blocking phosphorylation of S10H3 in Pdyn neurons did not affect mechanical sensation. Statistical analysis also revealed that there were no significant differences between the changes in AAV9_mutH3.1-treated hybrid mice compared to the corresponding values in the AAV9_control or sham-operated groups (see further details in Supplementary Table S4). There was a similar trend in PWL to mechanical forces applied to the paw in wild-type animals infected with the AAV9_mutH3.1 (n=2).

3.5. Acute chemosensation was influenced by the viral infection itself but mutant histone H3.1 as assessed by formalin-induced nocifensive behavior

Formalin test was chosen as a model to assess the effect of blocking phosphorylation of S10H3 on acute pain sensation (Bolcskei et al., 2005; Tjolsen et al., 1992). Intraplantar injection of formalin (5%; i.pl) evoked nocifensive behavior, in two phases depending on the participating peripheral components of the pain pathway (Bolcskei et al., 2005; Tjolsen et al., 1992). In the first phase (0-15 min; direct activation of primary sensory neurons) the total duration of nocifensive reactions of animals in the sham-operated, AAV9_mutH3.1- and AAV9_control treated groups were 23.97±2.0, 38.92±2.6, and 38.53±6.5 sec, respectively. Interestingly, in the second phase of the test (15-60 min which corresponds to the effect of the inflammatory mediators released, the values in the sham-operated, AAV9_mutH3.1- and AAV9_control treated groups were 224.01±32.7, 145.38±2.6 and 146.73±6.4 sec, respectively (Fig. 3d & Suppl. Fig. S2). Thus, while an almost 40% reduction was observed in the nocifensive responses among animals in the virus-treated groups (AAV9_mutH3.1. and AAV9_control) compared to the sham-operated animals, there was no significant difference between animals infected with the two types of AAV9 (Supplementary Table S4).

Thus, our data suggest that the response to formalin-induced acute pain was not affected by the S10A phenotype of histone H3.1 during the direct/early activation of sensory nerve terminals, nor during the release of acute inflammatory neuromodulators in the second phase.

3.6. Changes related to the mutant phenotype of histone H3.1 were not a consequence of the deterioration of the general health of the experimental animals

To monitor the general well-being of mice after the surgery, body weight was followed for 3 weeks, performing measurements before each behavioral assessment. The body weight of animals decreased slightly at day 7 in both the AAV9_mutH3.1. (to 95.8%±0.7) and in the AAV9_control (to 97.1%±0.7) groups, with no significant difference between them (Fig3e). By day 14 animals in both groups regained their baseline weight that was almost identical to those of the animals in the sham-operated group (Fig. 3e; for statistical analysis see Supplementary Table S4). There was a similar tendency in post-operative weight change in the case of the wild-type animals that had been infected with the AAV9_mutH3.1 (n=2). Interestingly, animals that received the AAV9_mutH3.1. virus intrathecally started to gain weight by the end of the third week, but the further investigation of this change was beyond the scope of this study and the experimental setup did not allow the follow-up of this weight change.

3.7. Intrathecal delivery of the viral constructs effectively transfects SDH neurons

Viral infection in the SDH of Pdyn::cas9-EGFP mice was confirmed with immunocytochemistry, 5 weeks after the intrathecal administration. Transverse sections from the lumbar spinal cord of the sacrificed and perfused animals were immunostained with antibodies against GFP and RFP that recognized the genetically encoded EGFP and mCherry proteins, respectively (Fig. 4).

Due to the cre-independency of mCherry expression in the AAV9_mutH3.1 vector, and the earlier reported tropism of AAV9 to glial cells when administered in the CSF (Murlidharan et al., 2014), non-Pdyn neurons and even non-neuronal cells occasionally also showed mCherry expression in the sections.

Animals in the AAV9_mutH3.1-treated group showed a granulated-looking red fluorescence indicating mCherry scattered in the entire dorsal horn. However, the granulated staining was almost confluent in the cytoplasm of cells located in the more superficial region (laminae I-II) of the dorsal horn (Fig. 4a). In deeper laminae (III-VI), the granulated mCherry signal was sparser resembling cytoplasmic dots around the nucleus labeled with DAPI (Fig. 4a). This staining pattern is probably due to the lower expression rate of mCherry in this construct, which is a known issue when CMV promoter is used to drive protein expression in adult neurons (Tenenbaum et al., 2004).

Localization and pattern of the enhanced mCherry signal in animals of the AAV9_control-treated group exhibited an almost identical pattern to that observed in their littermates infected with AAV9_mutH3.1 (Fig. 4b). The AAV9_control vector expresses mCherry as a fusion protein cre-dependently, thus, in theory, the mCherry signal should have been restricted to Pdyn-expressing neurons. However, mostly in the deeper laminae, some non-Pdyn cells still contained a weak mCherry fluorescence in a dotted fashion (Fig. 4b panel 2) that is likely the result of leakage expression of this bicistronic fusion protein.

Sections taken from animals in the sham-operated group had no mCherry signal anywhere in the spinal cord (Fig. 4c).

4. Discussion

We previously reported that Pdyn neurons had the largest share among p-S10H3-expressing neurons following burn injury both in wild-type and Pdyn::cas9-EGFP transgenic mice (Varga et al., 2021) suggesting their possible key involvement in the development of heat hyperalgesia after burn injury. Thus, in the present study, we tested the hypothesis that phosphorylation of S10H3 might be a crucial post-translational modification (PTM) in acute thermosensation, by combining the AAV system, dominant-negative approach, transgenic technology and CRISPR-based genome editing.

4.1. Validity of the Pdyn::cas9-EGFP transgenic model

Transgenic cre-recombinase expressing driver mice strains occasionally show inhomogeneity in the expression level of the enzyme among CNS regions that, otherwise, are known to contain the type of neuron tagged with the cre enzyme. Therefore, we first tested whether our selected Pdyn-IRES-cre strain is suitable for detecting Pdyn neurons in the spinal cord. The distribution of the reporter EGFP molecule in Pdyn::cas9-EGFP double heterozygous progenies showed close to identical expression pattern to the corresponding reference atlas (Allen Brain; www.brain-map.org (Lau and Suh, 2017)) in various regions of the brain. Moreover, double-labeling experiments showed that the large majority of EGFP expressing spinal dorsal horn cells in Pdyn::cas9-EGFP mice was also recognized by a specific antibody raised against Pdyn.

4.2. Cell-specific blocking of S10H3 phosphorylation as a precision tool for deciphering the role of this PTM in the complex function of Pdyn neurons

Histone H3 protein is encoded by twelve genes altogether in the mouse which code for two isoforms: H3.1 and H3.2. Among those 12 genes, four produce H3.1 transcripts according to the HISTome2 database (Shah et al., 2020). Posttranslational modification, including acetylation, phosphorylation, methylation of the core histone proteins plays an important role in the epigenetic regulation of transcription in eukaryotes (Hansen et al., 1998; Strahl and Allis, 2000). Phosphorylation of serine 10 in the N-terminal tail of histone H3 is not only involved in cell division in mitotic cells such as microglial cells but also participates in stimulus-dependent gene transcription in post-mitotic cells like neurons (Cheung et al., 2000; Prigent and Dimitrov., 2003), affecting only a certain subset of genes instead of the whole genome.

Given that this epigenetic tag is essential for survival (Prigent and Dimitrov, 2003), targeting histone phosphorylation with knockout technology is not an option. Due to multiple copies of histone H3.1 genes (Shah et al., 2020) to generate a viable “partially” knockout mouse (i.e. point-mutation at position serine 10 of histone H3.1) gene-editing had to be designed in such a way that it would be restricted to only a distinct subpopulation of SDH neurons, in our case Pdyn neurons. The AAV-CRISPR system proved suitable for in vivo genome editing in a cell-specific manner in non-dividing cells, such as postmitotic neurons (Lau and Suh, 2017). Thus, neuron-specific mutagenesis of histone H3.1 at position S10 via viral-based in vivo genome editing was utilized to achieve relatively long-term expression of CRISPR components. Recombinant AAV vectors for transgene delivery offer several advantages, such as tissue-specific serotypes, lack of immune response, low toxicity, minimal integration capacity, and high transduction efficiency (Lau and Suh, 2017; Senis et al., 2014). However, limited packaging size (up to 4.5kb) of the viral vector and the transient nature of the transgene expression is regarded as disadvantages of the use of AAVs (Chew et al., 2016; Lau and Suh, 2017; Senis et al., 2014). We managed to solve packaging by using cas9 expressing transgenic lines, the major hurdle of delivery of multicomponent CRISPR complex was circumvented. With this approach transgene expression is strictly controlled spatially on one hand by the cre-dependency of cas9 protein and on the other hand by administration of AAV-CRISPR virus directly into the subarachnoid space through a limited interval via an osmotic minipump. We believe that these measures minimized the probability of off-target mutagenesis and undesirable side effects of this AAV9-CRISPR-based strategy in organs other than the spinal cord (Lau and Suh, 2017).

4.3. Technical considerations

One important feature of our approach is the fact that cas9, whose expression otherwise is a rate-limiting step in the CRISPR/cas9 system, is available immediately after transduction with the virus due to the use of transgenic technology. It should be noted that long-term expression of cas9 may activate humoral immune response (Chew et al., 2016). Although phenotypic signs of off-target effects were undetectable, target mismatch tolerance of CRISPR/cas9 cannot be excluded (Kuscu et al., 2014; Yang et al., 2014). Together these might contribute to the slight degree of weight loss at 7 days after administration of the viruses via osmotic pump implantation. Further screening of CRISPR off-target effects was beyond the scope of this study.

The CRISPR/cas9 system with homolog-directed repair (HDR) could not be used in our approach as HDR functions inefficiently in postmitotic neurons (Hsu et al., 2014). Therefore, we used a dominant-negative technology in a combination with multiplex CRISPR/cas9-based genome editing for targeting the histone H3.1 gene in a single expression cassette. Using the multiple copies of U6 promoter to drive sgRNAs, one cannot rule out genetic recombination in the viral sequence (Vidigal and Ventura, 2015).

4.4. Putative parallel roles of spinal Pdyn neurons

Blocking histone H3.1 phosphorylation in Pdyn neurons specifically, by introducing the S10A mutation caused a significant and sustained elevation in the thermal nociceptive threshold that peaked at postoperative day 7. At the same time, neither mechanical sensitivity nor acute peripheral chemonociception to formalin was affected by blocking the same PTM. A robust confirmation of the role of Pdyn neurons was that wild-type C57/B6 mice injected with the AAV9_mutH3.1 showed no significant changes either in thermal or mechanical responses as S10A mutation integrated into Pdyn neurons only in a cre-dependent manner.

Several recent reports concluded that spinal Pdyn neurons play a role in gating mechanical pain (Brewer et al., 2020; Duan et al., 2014), while our results seemingly do not support these earlier findings. A possible explanation for this discrepancy comes from the different strategies by which the somatosensory dorsal horn neural network was targeted. With a chemogenic approach (Brewer et al., 2020; Duan et al., 2014) the entire spinal inhibitory pool of Pdyn interneurons was ablated/erased from the spinal sensory circuits that led to a reduced level of mechanosensation. In our experimental design, Pdyn neurons remained intact and fully functional in all other aspects except for a single PTM (phosphorylation of histone H3.1 on S10) and the consequential downstream target-derived actions. We have recently found that the majority of p-S10H3-expressing dynorphinergic neurons was Lmx1b-IR (83.3%) in laminae I-IIo following burn injury (Varga et al., 2021) suggesting that noxious thermal pain is probably processed by a distinct excitatory subgroup of Pdyn neurons in the SDH. In line with our observation, a recent comprehensive transcriptomics study revealed that the glutamatergic subset of Pdyn neurons mediates hyperalgesia induced by peripheral tissue damage in the rat (Sapio et al., 2021). Interestingly, it has been reported that thermosensitive neurons in the lateral parabrachial nucleus (LPb), a relay nucleus for ascending somatosensory pathway for pain, produce dynorphin (Geerling et al., 2016). As the mutation induced by our strategy stayed confined within the spinal cord, likely, spinal Pdyn neurons can also participate in acute thermosensation through strictly controlled epigenetic regulation/machinery. Thus, it seems very likely that the reported Pdyn-dependent suppression of mechanical sensitivity (Brewer et al., 2020; Duan et al., 2014) is regulated by other types of epigenetic mechanisms and that Pdyn neurons in the SDH contribute to the processing of more than one sensory modality while participating in the same anatomical circuit.

4.5. Selective mutation-based fine dissection of complex neuronal functions – future perspectives for the SDH

Combining novel biotechnological tools, we provided evidence for the importance of histone H3.1 phosphorylation at position S10 in Pdyn neuron in the response to painful thermal stimulation. In certain pathological pain states (inflammation or nerve injury) this neuro-epigenetic signal may be one of the molecular mechanisms that result in increased neuronal activity and hyperalgesic remodeling through permissive transcription of certain pain-related genes such as prodynorphin itself (Bagley and Ingram, 2020; Naranjo et al., 1991; Romero et al., 2012; Sapio et al., 2020; Sapio et al., 2021; Wang et al., 2001).

Pdyn neurons are members of the endogenous opioid releasing neurons that participate in the descending pain modulatory networks (Bagley and Ingram, 2020; Millan, 2002). Thus, it is reasonable to suggest that similar epigenetic tags on the same or other motifs may be equally important in the regulation of parallel functions of other neuronal types within the same system, such as enkephalinergic neurons.

A thorough description of the modulatory effects of different PTMs within the neurochemically discrete groups of SDH neurons upon different somatosensory modalities would be a necessary but tedious task. Nevertheless, we believe that this approach would explain some of the contradictory findings concerning the function of certain neuronal populations in the SDH and might shed light on how complex sensory processing of different modalities is solved with a limited number and variety of neurons within the SDH.

Figure 1

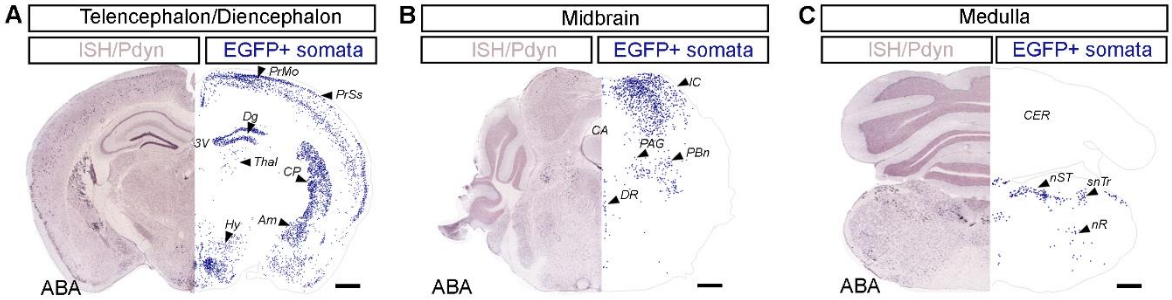

Immunohistochemical mapping revealed that regional distribution of dynorphinergic neurons in the brain of a Pdyn::cas9-EGFP mouse shows large similarity to the reference atlas provided by the Allen Institute

The distribution of Pdyn neurons was evaluated by plotting immunopositive cell bodies (revealed by the HRP/DAB method) through the telencephalon/diencephalon (A), the midbrain (B), and the medulla (C) of a Pdyn::cas9-EGFP mouse. On the right side of each panel, blue dots represent the location of Pdyn-immunopositive neurons, detected and reconstructed with the aid of Neurolucida (EGFP+ somata). The left side of each panel shows the corresponding reference image of in situ hybridization (ISH) data from the Allen Brain Atlas (ABA; (Lein et al., 2007)) displaying Pdyn mRNA expression pattern.

PrMo, primary motor area; PrSs, primary somatosensory area layer 2/3 and layer 5; Dg, dentate gyrus; Thal, mediodorsal nucleus of the thalamus; Hy, dorsomedial nucleus of the hypothalamus; CP, caudoputamen; Am, central amygdalar nucleus; 3V, third ventricle; IC, inferior colliculus; PAG, periaqueductal gray; PBn, parabrachial nucleus; DR, dorsal nucleus raphe; CA, cerebral aqueduct; CER, cerebellum; nST, nucleus of the solitary tract; snTr, spinal nucleus of the trigeminal; nR, reticular nucleus. Scale bar, 500 μm.

Figure 2

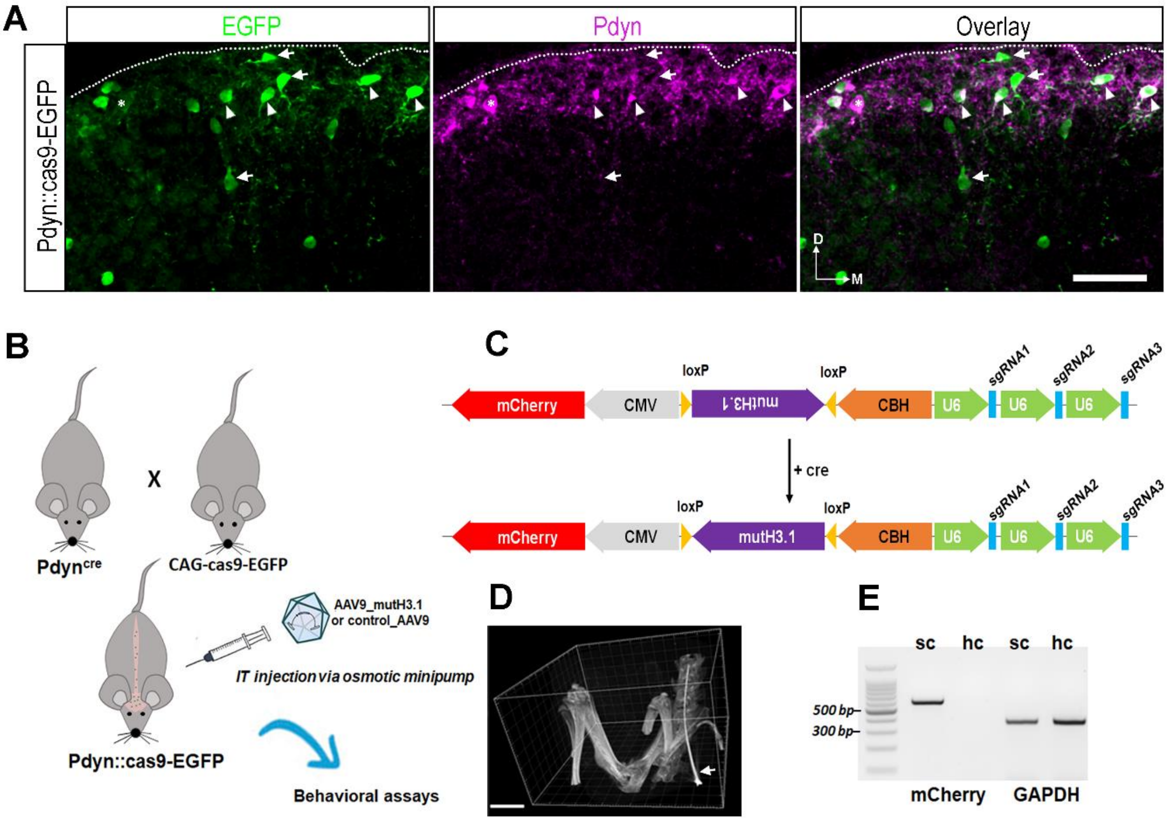

Cell-type specific targeted delivery of the necessary components for genome editing of histone H3.1 via CRISPR/cas9 strategy

A Immunostaining with antibodies against EGRP (green), Pdyn (magenta) in a projected image of seven optical sections with a 40x lens from a transverse spinal cord section of a Pdyn::cas9-EGFP mouse. The overlay shows a merged image. The numerous EGRP-immunoreactive neurons are predominantly visible in the superficial layers of the lumbar spinal cord. The majority of these are Pdyn+ (arrowheads), while some of them lack Pdyn (arrow). Few Pdyn-expressing neurons lack the EGFP signal (asterisk). D, dorsal; M, medial; Scale bar, 50 µm.

B Schematic drawing representing the CRISPR/cas9 strategy to establish the mutant histone H3.1 (mutH3.1) in Pdyn neurons. The abbreviation mutH3.1 refers to serine to alanine exchange (S10A) at position serine 10 of the wild-type histone H3.1. IT, intrathecal; AAV9_mutH3.1, the mutant histone H3.1-containing recombinant adeno-associated virus serotype 9.

C Schematic representation of the final insert synthesized and cloned into a recombinant AAV9. This cassette encoded mutH3.1 flanked by loxP sites (purple), three single guiding RNAs (sgRNAs; blue) driven by the human polymerase III U6 promoters (green), and a mCherry fluorescent protein (red). In this approach, S10A point mutation would be introduced into only cre-expressing neurons (i.e. into Pdyn-expressing neurons in Pdyn::cas9-EGFP hybrids). CMV, human cytomegalovirus (CMV) immediate early enhancer and promoter; CBH, chicken beta-actin promoter with CMV enhancer.

D 3D volume reconstruction of micro-CT images, used for validating the intrathecal position of the inserted cannule before the osmotic pump implantation. The intrathecal catheter (arrow) is shown within the subarachnoid space in a living deeply anesthetized Pdyn::cas9-EGFP mouse. The catheter was introduced at the level of L5-L6 vertebral laminae and pushed up to L1-L2. Scale bar, 5000 μm.

E In contrast to the hippocampus (hc), mCherry-specific RT-PCR produced a single sharp band in the spinal cord (sc) sample of a wild-type mouse that had been transfected with the AAV9_mutH3.1. GAPDH was amplified in both samples. BenchTop 100 bp DNA ladder was used as a reference.

Figure 3

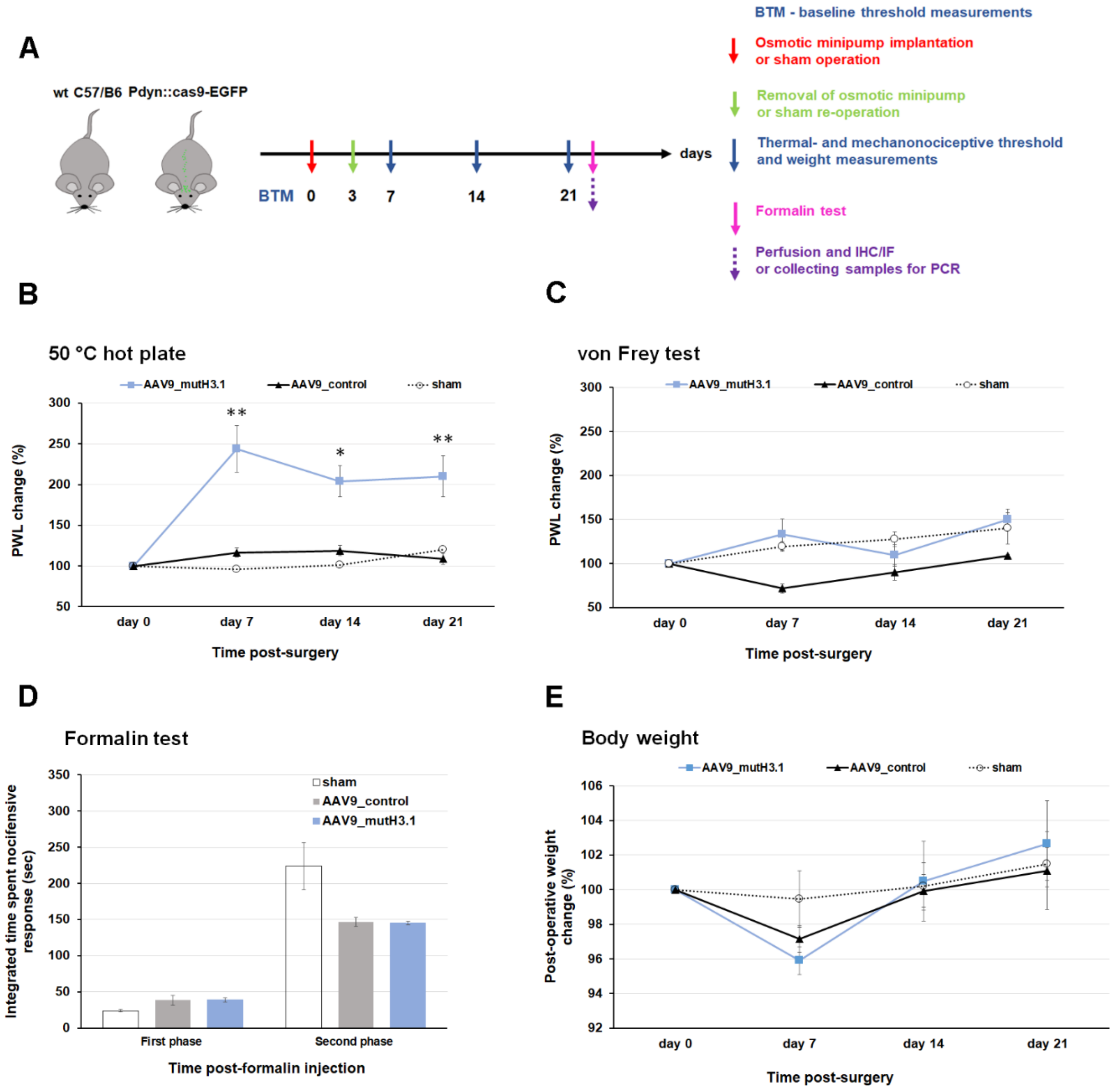

Intrathecal administration of AAV9_mutH3.1 into Pdyn::cas9-EGFP mice increases the thermal nociceptive threshold

A Schematic time scale of the experimental procedures. WT, wild-type C57Bl/6; IHC, immunohistochemistry; IF, immunofluorescent staining

B-C Changes in paw withdrawal latencies (PWL) to thermal- (B) and mechanical pain (C) were evaluated before (day 0) and after the surgery (day7, 14, 21) in different groups of Pdyn::cas9-EGFP mice (i.e. AAV9_mutH3.1, AAV9_control, sham-operated). Values at Day 0 represent the pre-surgery baseline values (BTM).

B AAV9_mutH3.1-treated animals exhibited higher thermal nociceptive threshold compared to the AAV9_control and sham operated groups at day 7. This significant elevation was persistent until the end of the observational period. (*p < 0.05 and **p < 0.01; see Supplementary Table S4).

C Paw withdrawal latency to painful mechanical stimuli showed no significant alterations within, and differences between the groups.

D Formalin-induced somatic pain was quantified as the integrated time spent exhibiting nocifensive behavioral during early (0-15 min) and late (15-60 min) phases of formalin application. Formalin-induced nocifensive behavior was reduced by 40% in the second phase in mice that had been infected with AAV9 irrespectively from their transgenes to be expressed, although, this reduction did not reach a statistically significant level.

E Changes in body weight were evaluated before (day 0) and after the surgery (day7, 14, 21) in different groups of Pdyn::cas9-EGFP mice (i.e. AAV9_mutH3.1, AAV9_control, sham-operated). Day 0 represents the pre-surgery baseline value. Transduction with the viruses (AAV9_mutH3.1 or AAV9_control) led to a modest body weight loss by day 7 that resolved later in all groups.

Figure 4

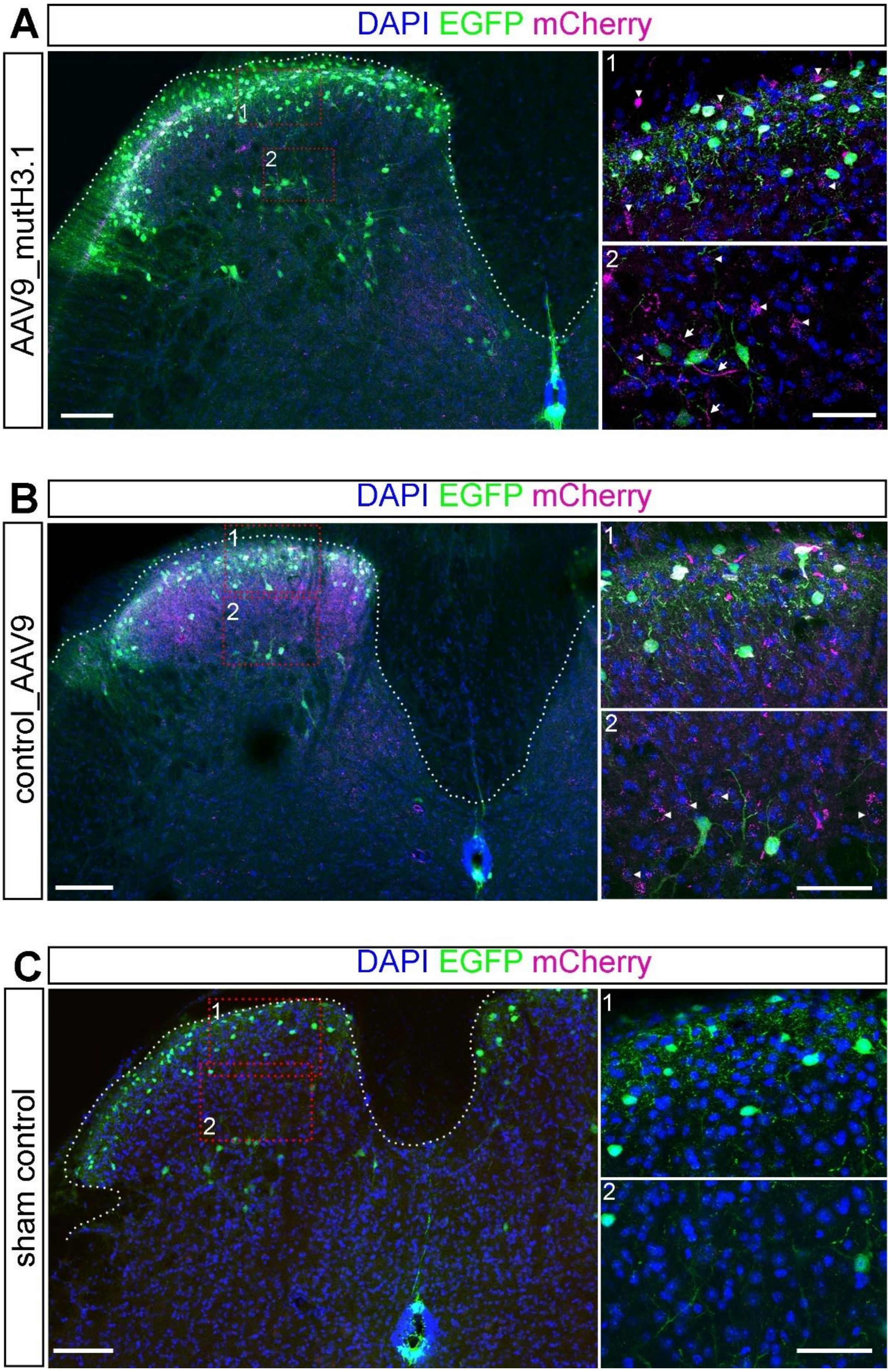
A
DAPI EGFP mCherry
AAV9_mutH3.1
1
2
1
2
B
DAPI EGFP mCherry
control_AAV9
1
2
1
2
C
DAPI EGFP mCherry
sham control
1
2
1
2

Widespread distribution of AAV9 viral particle in the spinal dorsal horn of Pdyn::cas9-EGFP mice as identified by the presence of mCherry tag encoded by the virus

Representative images showing immunostaining with antibodies against EGFP (green), mCherry (magenta), and DAPI (blue) in projected images of 4 optical sections taken with a 10x lens in the spinal cord from an AAV9_mutH3.1 vector treated (A), an AAV9_control treated (B) and a sham-operated (C) Pdyn::cas9-EGFP mouse. Insets (surrounded by red dotted line) from the superficial (1) and deeper (2) region of the SDH are Z-intensity projections, gathered with a 40x lens from 16 optical slices (each 0.5-µm-thick). White dotted lines on the left panels indicate borders between white and grey matter. Scale bar, 100 µm on A, B and C and 20 µm on the insets.

A Neurons showing mCherry-immunoreactivity are scattered throughout the SDH. Some Pdyn neurons (green to to their EGFP expression) show strong mCherry signal especially in the superficial region of the dorsal horn (inset 1). Non-Pdynergic dorsal horn cells show only moderate, dotted expression pattern of mCherry (insets 1&2; arrowhead). Prominent mCherry-positive protrusions, that lack EGFP and most likely belong to non-Pdyn neurons are also visible (inset 2; arrows).

B Administration of AAV9_control virus into Pdyn::cas9-EGFP mice produced an expression pattern of mCherry, similar to that shown in panel a. Arrowheads label non-Pdyn neurons exhibiting mCherry-specific immunoreaction (inset 2).

C The mCherry-specific fluorescent signal is completely missing in the transverse spinal cord sections of animals in the sham-operated group.

References

Bagley, E.E., Ingram, S.L., 2020. Endogenous opioid peptides in the descending pain modulatory circuit. Neuropharmacology 173, 108131.

Baseer, N., Polgar, E., Watanabe, M., Furuta, T., Kaneko, T., Todd, A.J., 2012. Projection neurons in lamina III of the rat spinal cord are selectively innervated by local dynorphin-containing excitatory neurons. J Neurosci 32, 11854-11863.

Bolcskei, K., Helyes, Z., Szabo, A., Sandor, K., Elekes, K., Nemeth, J., Almasi, R., Pinter, E., Petho, G., Szolcsanyi, J., 2005. Investigation of the role of TRPV1 receptors in acute and chronic nociceptive processes using gene-deficient mice. Pain 117, 368-376.

Boyle, K.A., Gutierrez-Mecinas, M., Polgar, E., Mooney, N., O'Connor, E., Furuta, T., Watanabe, M., Todd, A.J., 2017. A quantitative study of neurochemically defined populations of inhibitory interneurons in the superficial dorsal horn of the mouse spinal cord. Neuroscience 363, 120-133.

Brewer, C.L., Styczynski, L.M., Serafin, E.K., Baccei, M.L., 2020. Postnatal maturation of spinal dynorphin circuits and their role in somatosensation. Pain 161, 1906-1924.

Cheung, P., Allis, C.D., Sassone-Corsi, P., 2000. Signaling to chromatin through histone modifications. Cell 103, 263-271.

Chew, W.L., Tabebordbar, M., Cheng, J.K., Mali, P., Wu, E.Y., Ng, A.H., Zhu, K., Wagers, A.J., Church, G.M., 2016. A multifunctional AAV-CRISPR-Cas9 and its host response. Nat Methods 13, 868-874.

Descalzi, G., Ikegami, D., Ushijima, T., Nestler, E.J., Zachariou, V., Narita, M., 2015. Epigenetic mechanisms of chronic pain. Trends Neurosci 38, 237-246.

Doyle, A., McGarry, M.P., Lee, N.A., Lee, J.J., 2012. The construction of transgenic and gene knockout/knockin mouse models of human disease. Transgenic Res 21, 327-349.

Duan, B., Cheng, L., Bourane, S., Britz, O., Padilla, C., Garcia-Campmany, L., Krashes, M., Knowlton, W., Velasquez, T., Ren, X., Ross, S., Lowell, B.B., Wang, Y., Goulding, M., Ma, Q., 2014. Identification of spinal circuits transmitting and gating mechanical pain. Cell 159, 1417-1432.

Espejo, E.F., Mir, D., 1994. Differential effects of weekly and daily exposure to the hot plate on the rat's behavior. Physiol Behav 55, 1157-1162.

Geerling, J.C., Kim, M., Mahoney, C.E., Abbott, S.B., Agostinelli, L.J., Garfield, A.S., Krashes, M.J., Lowell, B.B., Scammell, T.E., 2016. Genetic identity of thermosensory relay neurons in the lateral parabrachial nucleus. Am J Physiol Regul Integr Comp Physiol 310, R41-54.

Hansen, J.C., Tse, C., Wolffe, A.P., 1998. Structure and function of the core histone N-termini: more than meets the eye. Biochemistry 37, 17637-17641.

Hook, V., Funkelstein, L., Lu, D., Bark, S., Wegrzyn, J., Hwang, S.R., 2008. Proteases for processing proneuropeptides into peptide neurotransmitters and hormones. Annu Rev Pharmacol Toxicol 48, 393-423.

Hsu, P.D., Lander, E.S., Zhang, F., 2014. Development and applications of CRISPR-Cas9 for genome engineering. Cell 157, 1262-1278.

Huang, J., Polgar, E., Solinski, H.J., Mishra, S.K., Tseng, P.Y., Iwagaki, N., Boyle, K.A., Dickie, A.C., Kriegbaum, M.C., Wildner, H., Zeilhofer, H.U., Watanabe, M., Riddell, J.S., Todd, A.J., Hoon, M.A., 2018. Circuit dissection of the role of somatostatin in itch and pain. Nat Neurosci 21, 707-716.

Huang, M., Huang, T., Xiang, Y., Xie, Z., Chen, Y., Yan, R., Xu, J., Cheng, L., 2008. Ptf1a, Lbx1 and Pax2 coordinate glycinergic and peptidergic transmitter phenotypes in dorsal spinal inhibitory neurons. Dev Biol 322, 394-405.

Kardon, A.P., Polgar, E., Hachisuka, J., Snyder, L.M., Cameron, D., Savage, S., Cai, X., Karnup, S., Fan, C.R., Hemenway, G.M., Bernard, C.S., Schwartz, E.S., Nagase, H., Schwarzer, C., Watanabe, M., Furuta, T., Kaneko, T., Koerber, H.R., Todd, A.J., Ross, S.E., 2014. Dynorphin acts as a neuromodulator to inhibit itch in the dorsal horn of the spinal cord. Neuron 82, 573-586.

Kohn, H.I., Kallman, R.F., 1957. The influence of strain on acute x-ray lethality in the mouse. II. Recovery rate studies. Radiat Res 6, 329-338.

Krashes, M.J., Shah, B.P., Madara, J.C., Olson, D.P., Strochlic, D.E., Garfield, A.S., Vong, L., Pei, H., Watabe-Uchida, M., Uchida, N., Liberles, S.D., Lowell, B.B., 2014. An excitatory paraventricular nucleus to AgRP neuron circuit that drives hunger. Nature 507, 238-242.

Kuscu, C., Arslan, S., Singh, R., Thorpe, J., Adli, M., 2014. Genome-wide analysis reveals characteristics of off-target sites bound by the Cas9 endonuclease. Nat Biotechnol 32, 677-683.

Lau, C.H., Suh, Y., 2017. In vivo genome editing in animals using AAV-CRISPR system: applications to translational research of human disease. F1000Res 6, 2153.

Lein, E.S., Hawrylycz, M.J., Ao, N., Ayres, M., Bensinger, A., Bernard, A., Boe, A.F., Boguski, M.S., Brockway, K.S., Byrnes, E.J., Chen, L., Chen, L., Chen, T.M., Chin, M.C., Chong, J., Crook, B.E., Czaplinska, A., Dang, C.N., Datta, S., Dee, N.R., Desaki, A.L., Desta, T., Diep, E., Dolbeare, T.A., Donelan, M.J., Dong, H.W., Dougherty, J.G., Duncan, B.J., Ebbert, A.J., Eichele, G., Estin, L.K., Faber, C., Facer, B.A., Fields, R., Fischer, S.R., Fliss, T.P., Frensley, C., Gates, S.N., Glattfelder, K.J., Halverson, K.R., Hart, M.R., Hohmann, J.G., Howell, M.P., Jeung, D.P., Johnson, R.A., Karr, P.T., Kawal, R., Kidney, J.M., Knapik, R.H., Kuan, C.L., Lake, J.H., Laramee, A.R., Larsen, K.D., Lau, C., Lemon, T.A., Liang, A.J., Liu, Y., Luong, L.T., Michaels, J., Morgan, J.J., Morgan, R.J., Mortrud, M.T., Mosqueda, N.F., Ng, L.L., Ng, R., Orta, G.J., Overly, C.C., Pak, T.H., Parry, S.E., Pathak, S.D., Pearson, O.C., Puchalski, R.B., Riley, Z.L., Rockett, H.R., Rowland, S.A., Royall, J.J., Ruiz, M.J., Sarno, N.R., Schaffnit, K., Shapovalova, N.V., Sivisay, T., Slaughterbeck, C.R., Smith, S.C., Smith, K.A., Smith, B.I., Sodt, A.J., Stewart, N.N., Stumpf, K.R., Sunkin, S.M., Sutram, M., Tam, A., Teemer, C.D., Thaller, C., Thompson, C.L., Varnam, L.R., Visel, A., Whitlock, R.M., Wohnoutka, P.E., Wolkey, C.K., Wong, V.Y., Wood, M., Yaylaoglu, M.B., Young, R.C., Youngstrom, B.L., Yuan, X.F., Zhang, B., Zwingman, T.A., Jones, A.R., 2007. Genome-wide atlas of gene expression in the adult mouse brain. Nature 445, 168-176.

Liang, D.Y., Sun, Y., Shi, X.Y., Sahbaie, P., Clark, J.D., 2014. Epigenetic regulation of spinal cord gene expression controls opioid-induced hyperalgesia. Mol Pain 10, 59.

Liang, L., Tao, Y.X., 2018. Expression of acetyl-histone H3 and acetyl-histone H4 in dorsal root ganglion and spinal dorsal horn in rat chronic pain models. Life Sci 211, 182-188.

Marvizon, J.C., Chen, W., Murphy, N., 2009. Enkephalins, dynorphins, and beta-endorphin in the rat dorsal horn: an immunofluorescence colocalization study. J Comp Neurol 517, 51-68.

Millan, M.J., 2002. Descending control of pain. Prog Neurobiol 66, 355-474.

Milne, R.J., Gamble, G.D., Holford, N.H., 1989. Behavioural tolerance to morphine analgesia is supraspinally mediated: a quantitative analysis of dose-response relationships. Brain Res 491, 316-327.

Murlidharan, G., Samulski, R.J., Asokan, A., 2014. Biology of adeno-associated viral vectors in the central nervous system. Front Mol Neurosci 7, 76.

Naranjo, J.R., Mellstrom, B., Achaval, M., Sassone-Corsi, P., 1991. Molecular pathways of pain: Fos/Jun-mediated activation of a noncanonical AP-1 site in the prodynorphin gene. Neuron 6, 607-617.

Petitjean, H., Pawlowski, S.A., Fraine, S.L., Sharif, B., Hamad, D., Fatima, T., Berg, J., Brown, C.M., Jan, L.Y., Ribeiro-da-Silva, A., Braz, J.M., Basbaum, A.I., Sharif-Naeini, R., 2015. Dorsal Horn Parvalbumin Neurons Are Gate-Keepers of Touch-Evoked Pain after Nerve Injury. Cell Rep 13, 1246-1257.

Platt, R.J., Chen, S., Zhou, Y., Yim, M.J., Swiech, L., Kempton, H.R., Dahlman, J.E., Parnas, O., Eisenhaure, T.M., Jovanovic, M., Graham, D.B., Jhunjhunwala, S., Heidenreich, M., Xavier, R.J., Langer, R., Anderson, D.G., Hacohen, N., Regev, A., Feng, G., Sharp, P.A., Zhang, F., 2014. CRISPR-Cas9 knockin mice for genome editing and cancer modeling. Cell 159, 440-455.

Plone, M.A., Emerich, D.F., Lindner, M.D., 1996. Individual differences in the hotplate test and effects of habituation on sensitivity to morphine. Pain 66, 265-270.

Prigent, C., Dimitrov, S., 2003. Phosphorylation of serine 10 in histone H3, what for? J Cell Sci 116, 3677-3685.

Romero, A., Gonzalez-Cuello, A., Laorden, M.L., Campillo, A., Vasconcelos, N., Romero-Alejo, E., Puig, M.M., 2012. Effects of surgery and/or remifentanil administration on the expression of pERK1/2, c-Fos and dynorphin in the dorsal root ganglia in mice. Naunyn Schmiedebergs Arch Pharmacol 385, 397-409.

Sapio, M.R., Iadarola, M.J., Loydpierson, A.J., Kim, J.J., Thierry-Mieg, D., Thierry-Mieg, J., Maric, D., Mannes, A.J., 2020. Dynorphin and Enkephalin Opioid Peptides and Transcripts in Spinal Cord and Dorsal Root Ganglion During Peripheral Inflammatory Hyperalgesia and Allodynia. J Pain 21, 988-1004.

Sapio, M.R., Kim, J.J., Loydpierson, A.J., Maric, D., Goto, T., Vazquez, F.A., Dougherty, M.K., Narasimhan, R., Muhly, W.T., Iadarola, M.J., Mannes, A.J., 2021. The Persistent Pain Transcriptome: Identification of Cells and Molecules Activated by Hyperalgesia. J Pain.

Sardella, T.C., Polgar, E., Garzillo, F., Furuta, T., Kaneko, T., Watanabe, M., Todd, A.J., 2011. Dynorphin is expressed primarily by GABAergic neurons that contain galanin in the rat dorsal horn. Mol Pain 7, 76.

Sato, F., Sasaki, S., Kawashima, N., Chino, F., 1981. Late effects of whole or partial body x-irradiation on mice: life shortening. Int J Radiat Biol Relat Stud Phys Chem Med 39, 607-615.

Schmidtko, A., Luo, C., Gao, W., Geisslinger, G., Kuner, R., Tegeder, I., 2008. Genetic deletion of synapsin II reduces neuropathic pain due to reduced glutamate but increased GABA in the spinal cord dorsal horn. Pain 139, 632-643.

Senis, E., Fatouros, C., Grosse, S., Wiedtke, E., Niopek, D., Mueller, A.K., Borner, K., Grimm, D., 2014. CRISPR/Cas9-mediated genome engineering: an adeno-associated viral (AAV) vector toolbox. Biotechnol J 9, 1402-1412.

Shah, S.G., Mandloi, T., Kunte, P., Natu, A., Rashid, M., Reddy, D., Gadewal, N., Gupta, S., 2020. HISTome2: a database of histone proteins, modifiers for multiple organisms and epidrugs. Epigenetics Chromatin 13, 31.

Strahl, B.D., Allis, C.D., 2000. The language of covalent histone modifications. Nature 403, 41-45.

Tenenbaum, L., Chtarto, A., Lehtonen, E., Velu, T., Brotchi, J., Levivier, M., 2004. Recombinant AAV-mediated gene delivery to the central nervous system. J Gene Med 6 Suppl 1, S212-222.

Tjolsen, A., Berge, O.G., Hunskaar, S., Rosland, J.H., Hole, K., 1992. The formalin test: an evaluation of the method. Pain 51, 5-17.

Tochiki, K.K., Maiaru, M., Norris, C., Hunt, S.P., Geranton, S.M., 2016. The mitogen and stress-activated protein kinase 1 regulates the rapid epigenetic tagging of dorsal horn neurons and nocifensive behaviour. Pain 157, 2594-2604.

Torres-Perez, J.V., Santha, P., Varga, A., Szucs, P., Sousa-Valente, J., Gaal, B., Sivado, M., Andreou, A.P., Beattie, S., Nagy, B., Matesz, K., JS, C.A., Jancso, G., Nagy, I., 2017. Phosphorylated Histone 3 at Serine 10 Identifies Activated Spinal Neurons and Contributes to the Development of Tissue Injury-Associated Pain. Sci Rep 7, 41221.

van den Pol, A.N., 2012. Neuropeptide transmission in brain circuits. Neuron 76, 98-115.

Varga, A., Meszar, Z., Sivado, M., Bacskai, T., Vegh, B., Kokai, E., Nagy, I., Szucs, P., 2021. Spinal Excitatory Dynorphinergic Interneurons Contribute to Burn Injury-Induced Nociception Mediated by Phosphorylated Histone 3 at Serine 10 in Rodents. Int J Mol Sci 22.

Vidigal, J.A., Ventura, A., 2015. Rapid and efficient one-step generation of paired gRNA CRISPR-Cas9 libraries. Nat Commun 6, 8083.

Wang, Z., Gardell, L.R., Ossipov, M.H., Vanderah, T.W., Brennan, M.B., Hochgeschwender, U., Hruby, V.J., Malan, T.P., Jr., Lai, J., Porreca, F., 2001. Pronociceptive actions of dynorphin maintain chronic neuropathic pain. J Neurosci 21, 1779-1786.

Willekens, I., Buls, N., Lahoutte, T., Baeyens, L., Vanhove, C., Caveliers, V., Deklerck, R., Bossuyt, A., de Mey, J., 2010. Evaluation of the radiation dose in micro-CT with optimization of the scan protocol. Contrast Media Mol Imaging 5, 201-207.

Yang, L., Grishin, D., Wang, G., Aach, J., Zhang, C.Z., Chari, R., Homsy, J., Cai, X., Zhao, Y., Fan, J.B., Seidman, C., Seidman, J., Pu, W., Church, G., 2014. Targeted and genome-wide sequencing reveal single nucleotide variations impacting specificity of Cas9 in human stem cells. Nat Commun 5, 5507.

Deviations from the personal composition and the cost plan, their reasons and impact on the research process:

Alteration in personal composition of the project was neccessary due to my advanced allergy to rodents. Despite wearing protective clothing and taking preventive medication, unfortunatelly, I was not able to keep contact with the laboratory mice because of my severe allergic reaction to these animals. That is why participation of the following collegues - who all had been eager to work in it - was necessary for the outcome of the project:

Mihály Zoltán Mészár, PhD • intrathecal injection of viral CRISPR components through an osmotic pump into anesthetized mice. • statistical analysis of in vivo behavioral data.
Éva Kókai • immunohistochemistry • reconstructions on coronal brain sections using the Neurolucida program
Rita Varga Vidáné • performed in vivo behavioral tests (measurement of mechanosensitivity) in transgenic and wild-type mice
László Ducza • performed in vivo behavioral tests (measurement of mechanosensitivity) in transgenic and wild-type mice
Tímea Molnár Nánásiné • performed in vivo behavioral tests (preconditioning and hot plate test) and recorded all behavioural data obtained in our local database.

Due to covid 19 pandemics, international conferences were missed. Therefore, the amount that had been allocated to the conferences (daily fee, accommodation in abroad, registration fee and travel costs) was re-allocated to salary supplements to the coworkers (see above) who I had requested to join and carry out specific tasks in the frame of the project.